

# GreedyFool: An Imperceptible Black-box Adversarial Example Attack against Neural Networks

Hui Liu  
Wuhan University  
Penn State University

Bo Zhao  
Wuhan University

Jiabao Guo  
Wuhan University

Pengyuan Zhao  
Wuhan University

Peng Liu  
Penn State University

**Abstract**—Deep neural networks (DNNs) are inherently vulnerable to well-designed input samples called adversarial examples. The adversary can easily fool DNNs by adding slight perturbations to the input. In this paper, we propose a novel black-box adversarial example attack named GreedyFool, which synthesizes adversarial examples based on the differential evolution and the greedy approximation. The differential evolution is utilized to evaluate the effects of perturbed pixels on the confidence of the DNNs-based classifier. The greedy approximation is an approximate optimization algorithm to automatically get adversarial perturbations. Existing works synthesize the adversarial examples by leveraging simple metrics to penalize the perturbations, which lack sufficient consideration of the human visual system (HVS), resulting in noticeable artifacts. In order to sufficient imperceptibility, we launch a lot of investigations into the HVS and design an integrated metric considering just noticeable distortion (JND), Weber-Fechner law, texture masking and channel modulation, which is proven to be a better metric to measure the perceptual distance between the benign examples and the adversarial ones. The experimental results demonstrate that the GreedyFool has several remarkable properties including black-box, 100% success rate, flexibility, automation and can synthesize the more imperceptible adversarial examples than the state-of-the-art pixel-wise methods.

**Keywords**—deep neural networks, adversarial examples, differential evolution, greedy approximation, human visual system

## I. INTRODUCTION

Deep neural networks (DNNs) [1-3] have demonstrated impressive performance in wide application, e.g., image processing [4, 5], nature language processing [6, 7], speech recognition [8, 9], etc. Especially in the field of image classification, DNNs-based approach achieves even human-competitive results. These applications have a common characteristic: the adversary is able to impersonate a benign user to precisely control the input to DNNs-based services. However, recent studies found that DNNs are inherently vulnerable to well-designed input samples called adversarial examples. The attackers can easily fool DNNs by adding slight perturbations to the benign examples. Such attacks are a serious threat for those safety-critical systems, such as facial biometric systems [10], digital watermarking [11], etc. For example, the attacker who wears a pair of perturbed eyeglass frames could evade being recognized or impersonate another individual by the state-of-the-art face-recognition algorithm. In digital watermarking field, the adversarial perturbations could impact the integrity of the embedded pattern, making the watermark undetectable and the authenticity of the digital media unverifiable. The phenomena of adversarial example attacks have aroused great concern from academia and industry.

In image classification tasks, adversarial example attacks aim to mislead the DNNs-based classifier to the modified image as a wrong or specific target class. Generating adversarial examples could be formalized as an optimization

problem with constraints. This problem involves two aspects: how to solve for this optimal solution and how to define the perceptual loss.

Due to non-linear and non-convex of the DNN model, optimization problem of adversarial examples is difficult to solve. In recent years, many advanced solutions have been proposed. Szegedy C et al. [12] first revealed the sensitivity to well-designed perturbation which can be crafted by several gradient-based algorithms using back-propagation for obtaining gradient information. Specifically, Goodfellow I.J et al. [13] proposed the fast gradient sign method (FGSM) to yield a simple and fast method of generating adversarial examples based on a hypothesis in which the linearity and high-dimensions of inputs are the main reason why a broad class of networks are sensitive to small perturbation. Jacobian-based saliency map attack [14] is an efficient method to generate adversarial examples using forward-propagation, which compute the Jacobian of the input example and construct adversarial saliency maps to evaluate the effect of perturbed features. These approaches that require inner information of target DNNs, such as gradient information and network structures, cannot be applied to black-box attack scenarios. In one-pixel attack [15], Su J et al. proposed a black-box method for generating one-pixel adversarial perturbations based on the differential evolution, which requires only probability labels but no inner information of target DNNs and can attack more types of DNNs. However, when synthesizing adversarial examples, the attackers have no way of knowing in advance how many pixels may be perturbed, resulting in the failure of adversarial example attacks toward images.

In terms of the perceptual loss, most of the existing attacks utilize perceptual distance of  $L_p$  norms ( $L_0$ ,  $L_2$  and  $L_\infty$  norms) as constraint to penalize the perturbations. For example, Papernot N et al. [16] generated adversarial examples based on a precise understanding of the mapping between inputs and outputs of DNNs by  $L_2$  norm. FGSM [13] computed one-step gradient to synthesize adversarial examples by  $L_\infty$  norm. Carlini N et al. [17] used three distance metrics  $L_0$ ,  $L_2$  and  $L_\infty$  to quantify similarity. These metrics treat perturbations of different pixels in an image equally important for human eyes. However, visibility of perturbations is the perceived response by the individual to the physical stimulus. The measurement of the perceptual distance between the benign examples and the adversarial ones should take full consideration of the human visual system (HVS). Therefore, we launch a lot of investigations into the HVS and summarize four primary factors affecting the human vision: (a) Just noticeable distortion (JND) [18, 19]. Human eyes cannot sense a stimulus below the JND, which quantifies the sensitivity of the HVS to different background luminance. (b) Weber-Fechner law [20, 21]. The HVS is sensitive to luminance contrast rather than absolute luminance value. The Weber-Fechner law revealed important principle in psychophysics, which describes the logarithmic mapping between the magnitude of a physical

stimulus and its perceived intensity. (c) Texture masking [22]. Imperceptibility of perturbations is caused by an increase in the texture non-uniformity in the neighborhood. Human eyes are more sensitive to perturbations on pixels in smooth regions than those in textured regions. (d) Channel modulation [23, 24]. The strength of the signal in each channel would be proportional to the sensitivity of the human eye to it. And human vision has different sensitivity to the same perturbation in different color channels. These factors reveal the sensitivity of human eyes to pixel perturbations from four different aspects. There are many works introducing the HVS to quantify the perceptual loss. A typical work is that Luo B [22] defined perturbation sensitivity distance (PSD), taking the HVS into consideration, to measure perceptual distance between the benign examples and the adversarial ones. This method ignores the logarithmic mapping between the physical magnitude and its perceived intensity, and lacks consideration of the discrimination in different color channels. Our work integrates JND, Weber-Fechner law, texture masking and channel modulation and design a better metric to measure the perceptual loss caused by adversarial perturbations.

In this paper, we focus on the approach of synthesizing adversarial examples and the definition of the perceptual loss. To synthesize adversarial examples with no inner information of target DNNs, we apply the differential evolution [15, 25, 26] to evaluate the effects of perturbed pixels on the confidence of target DNNs and introduce the greedy approximation [22] to automatically find which pixels to perturb and what magnitude to modify effectively. In terms of the perceptual loss, previous related works used simple metrics to evaluate the perceptual distances between the benign examples and the adversarial ones, which could be easily detected by human eyes. We investigate the HVS and summarize four primary factors (JND, Weber-Fechner law, texture masking and channel modulation) affecting the human vision. Furthermore, we propose a comprehensive metric considering the HVS to evaluate the perceptual similarity between the benign examples and the adversarial ones. The experimental results prove that the GreedyFool can effectively synthesize the adversarial examples with low visibility and high success rate.

The paper makes the following contributions:

- (1) We investigate and discover that JND, Weber-Fechner law, texture masking and channel modulation are four primary factors affecting the human vision in the image domain.
- (2) We propose a black-box adversarial example attack approach GreedyFool, which requires only the feedback of the DNNs-based classifier but no inner information of target DNNs. Thus, the GreedyFool can attack more types of DNNs even if they are not differentiable.
- (3) We apply the differential evolution to evaluate the effects of pixel-wise perturbation and generate candidates with the higher perturbation priority, combining with the greedy approximation to automatically find which pixels to perturb and what magnitude to add. The proposed method achieves 100% success rate for non-targeted attacks and targeted attacks.
- (4) We design an integrated metric considering JND, Weber-Fechner law, texture masking and channel modulation of the HVS to evaluate the perceptual distances between the benign examples and the adversarial ones. The experimental

results show that the proposed perceptual loss is a better metric than the exiting pixel-wise metrics.

The remainder of this paper is organized as follows. We present the preliminaries in Section II and give the careful investigation into the HVS in Section III. In Section IV, we give details about design and implementation of the GreedyFool. The experimental evaluations are presented in Section V. Finally, we discuss several remarkable properties of the GreedyFool in Section VI and conclude the paper in Section VII.

## II. PRELIMINARIES

### A. Deep Neural Network

Deep neural network [1-3] is usually constructed by multiple neural network layers, which would be convolutional layers, pooling layers and fully connected layers as in convolutional neural network. A neural network layer consists of a set of perceptrons and each perceptron has multiple inputs and one output with an activation function, e.g., Sigmoid, ReLU. It can be formalized in a chain.

$$f(x, \theta) = f^{(k)}(\dots f^{(2)}(f^{(1)}(x, \theta_1), \theta_2), \theta_k) \quad (1)$$

where  $f^{(i)}(x, \theta_i)$  is the function of the  $i$ 'th layer of the network,  $i = 1, 2, \dots, k$ .  $x$  is the input example and  $\theta_i$  is the weight of the  $i$ 'th layer.

Among neural network architectures, residual network (ResNet) [2] and dense convolutional network (DenseNet) [3] are two types of widely used neural networks in image classification tasks. Instead of learning unreferenced functions, ResNet reformulates the layers as learning residual functions with reference to the layer inputs. A residual block is realized by feed-forward neural networks with "shortcut connections" shown in Fig. 1.

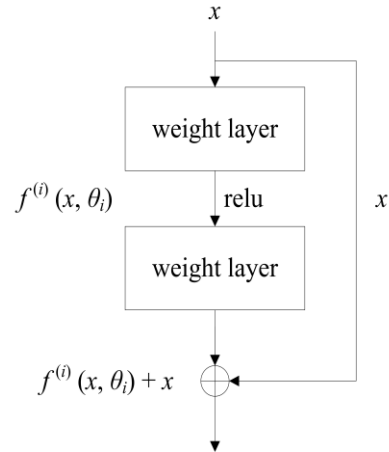


Fig. 1. A building block of residual learning. Shortcut connections are those skipping one or more layers.

We construct and train ResNet model as described in TABLE I, which has 470,218 parameters and performs 92.69% accuracy in CIFAR-10.

To further improve the information flow between layers, DenseNet connects each layer to every other layer in a feed-forward fashion. Layers between dense blocks are named as transition layers and change feature-map sizes via convolution and pooling. DenseNet model has 850,606 parameters and performs 94.28% accuracy in CIFAR-10, whose structure is described in TABLE II.

TABLE I. THE STRUCTURE OF RESNET MODEL.

Layer	Parameters
Convolution layer 1	kernel = 3, stride = 1, depth = 16
Residual block 1	$\begin{bmatrix} 3 \times 3, & 16 \\ 3 \times 3, & 16 \end{bmatrix} \times 5$
Residual block 2	$\begin{bmatrix} 3 \times 3, & 32 \\ 3 \times 3, & 32 \end{bmatrix} \times 5$
Residual block 3	$\begin{bmatrix} 3 \times 3, & 64 \\ 3 \times 3, & 64 \end{bmatrix} \times 5$
Global average pool	
Softmax classifier	

TABLE II. THE STRUCTURE OF DENSENET MODEL.

Layer	Parameters
Convolution layer 1	kernel = 3, stride = 1, depth = 24s
Dense block 1	$\begin{bmatrix} 1 \times 1, & 48 \\ 3 \times 3, & 12 \end{bmatrix} \times 16$
Transition layer 1	Convolution layer (kernel = 1, stride = 1, depth = 12) Average pooling layer (kernel = 2, stride = 2)
Dense block 2	$\begin{bmatrix} 1 \times 1, & 48 \\ 3 \times 3, & 12 \end{bmatrix} \times 16$
Transition layer 2	Convolution layer (kernel = 1, stride = 1, depth = 12) Average pooling layer (kernel = 2, stride = 2)
Dense block 3	$\begin{bmatrix} 1 \times 1, & 48 \\ 3 \times 3, & 12 \end{bmatrix} \times 16$
Transition layer 3	Convolution layer (kernel = 1, stride = 1, depth = 12) Average pooling layer (kernel = 2, stride = 2)
Global average pool	
Softmax classifier	

### B. CIFAR-10

The CIFAR-10 dataset consists of 60,000  $32 \times 32 \times 3$  color images, including 50,000 training images and 10,000 test images. It has 10 classes, including airplane, automobile, bird, cat, deer, dog, frog, horse, ship and truck, with 6,000 images per class. Due to its simplicity and small size, CIFAR-10 is easy to attack and defend. Therefore, CIFAR-10 is one of the most widely used image datasets to evaluate adversarial example attacks. In the paper, we adopt CIFAR-10 for the experiments and analyses.

### C. Adversarial Example Attacks

Adversarial example attacks aim to mislead a deep neural network to an incorrect label by adding small perturbations in the benign examples, even if the perturbations are barely recognizable by human eyes. Adversarial examples [1, 19] would be formulated as a box-constrained optimization problem. That is,

$$\begin{aligned}
 & \min \|\delta\|_p \\
 & s.t. \ f(X') = l' \\
 & \quad f(X) = l \\
 & \quad l' \neq l \\
 & \quad X' = X + \delta \in D
 \end{aligned} \tag{2}$$

where a trained DNN model  $f$  predicts the benign example  $X$  and the adversarial example  $X'$  into  $l$  and  $l'$  denotes the perceptual distance between two examples,  $\delta$  denotes the perturbation matrix added to the benign example for synthesizing the adversarial one, that remains in the benign domain  $D$ . This optimization problem minimizes the perturbation while misleading the DNN model to incorrect prediction.

### D. Perceptual Distance

The perceptual distance is utilized for measuring the perceptual similarity between the benign image and the adversarial image. Existing works mainly apply  $L_p$  norms (e.g.  $L_0$ ,  $L_2$  and  $L_\infty$ ) to measure the magnitude of perturbation  $\delta$  [1, 16, 17]. That is,

$$\|\delta\|_p = \left( \sum_{i=1}^n |\delta_i|^p \right)^{\frac{1}{p}} \tag{3}$$

where  $L_0$  norm counts the number of pixels perturbed in an image.  $L_2$  measures the Euclidean distance between the benign example and the adversarial example.  $L_\infty$  norm denotes the maximum for all vector elements  $|\delta_i|$ :  $\|\delta\|_\infty = \max(|\delta_i|)$ . The small  $L_p$  norm value indicates the more imperceptibility of perturbations. These metrics are objective, which treat perturbations of different pixels equally in an image. In fact, imperceptibility is the perceived response by the individual to the physical stimulus. Therefore, the mapping between physical stimulus and psychological perception should be fully considered in perceptual distance.

### E. Differential Evolution

Differential evolution [15, 25, 26] is a population-based optimization algorithm for solving complex optimization problems. By remembering individual optimal solution and sharing information within the population, the differential evolution solves the optimization problem through cooperation and competition among individuals within the population. The differential evolution algorithm is a simple real parameter optimization based on mutation, crossover and selection. Figure 2 presents its mechanism through a simple cycle of stages.

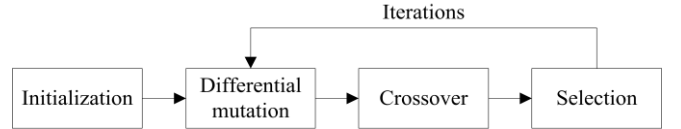


Fig. 2. Main stage of the differential evolution includes mutation, crossover and selection.

Due to non-linear and non-convex characteristics of the DNN model  $f$ , the Equation (2) is difficult to solve. It is proved that the differential evolution could efficiently find global optima than gradient-based methods or even other kinds of evolution algorithms [25]. The differential evolution is defined in Equation (4).

$$x_i(g+1) = x_{r1}(g) + F(x_{r2}(g) - x_{r3}(g)), \quad r1 \neq r2 \neq r3 \tag{4}$$

where  $r1$ ,  $r2$ ,  $r3$  are random numbers and  $F$  is the scale parameter set to 0.5. Three candidate solutions  $x_{r1}(g)$ ,  $x_{r2}(g)$  and  $x_{r3}(g)$  from the  $g$ 'th generation are randomly chosen to generate a new candidate solution  $x_i(g+1)$  of the  $g+1$ 'th generation. In this paper, the initial number of candidate solutions is 300, and at each iteration, another 300 candidate solutions will be produced by the differential evolution formula. The differential evolution neither requires the inner information of target DNNs, such as gradient information and network structures, nor requires the optimization problem to be differential as is required by classical optimization methods, e.g., gradient descent, quasi-newton, etc. Thus, these inherent features of the differential

evolution make the GreedyFool flexible, which is applicable to more types of DNNs as a black-box attack tool.

### III. HUMAN VISUAL SYSTEM

Human visual system is a multichannel model with characteristics of multi-frequency channel decomposition. Especially, the sensitivity of human eyes to perturbations is affected by several factors. We investigate the HVS and summarize four primary factors affecting the human vision in the image domain: JND, Weber-Fechner law, texture masking and channel modulation.

#### A. Just Noticeable Distortion

It is known that human eyes cannot perceive a stimulus below the just noticeable distortion [18, 19] threshold around a pixel in images. The sensitivity of human eyes to noise of images has negative correlation with JDN. The larger value of the JDN threshold indicates the more noise can be hidden. An appropriate JND model can significantly improve the performance in image processing tasks. The visibility threshold of the JND is formulated in Equation (5), curved in Fig. 3.

$$jnd(x, y) = \begin{cases} 17(1 - \sqrt{\frac{\bar{I}_{n \times n}(x, y)}{127}}) + 3, & \text{if } \bar{I}_{n \times n}(x, y) \leq 127 \\ \frac{3}{128}(\bar{I}_{n \times n}(x, y) - 127) + 3, & \text{otherwise} \end{cases} \quad (5)$$

where  $\bar{I}_{n \times n}(x, y)$  denotes the maximum luminance among a  $n \times n$  window at the coordinate  $(x, y)$ . Especially, we set  $n = 3$  and calculate the maximum luminance of the  $(x, y)$  pixel and its 8 neighbors.

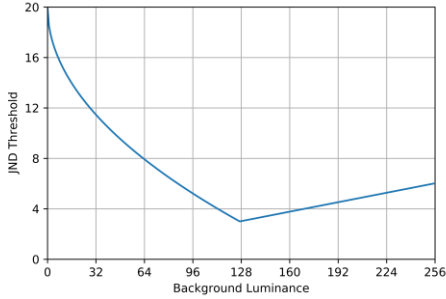


Fig. 3. Illustration of the JND. When the maximum luminance is 127, the JND threshold gets a minimum 3.

Figure 3 reveals the nonlinear relationship between the JND threshold and the maximum background luminance. Even if the magnitude of perturbations is the same, there are significant differences in perceived intensity of human eyes

under different luminance backgrounds. When the maximum luminance among a  $n \times n$  window lies in the interval  $[0, 127]$ , the JDN threshold decreases as the background luminance increases. When the maximum luminance among a  $n \times n$  window lies in the interval  $[127, 255]$ , the JDN threshold increases as the background luminance increases. If the maximum luminance is 127, the JDN threshold gets a minimum value 3. That indicates the perturbation at this coordinate is most easily perceived by the human eye.

#### B. Weber-Fechner Law

Weber-Fechner law [20, 21] has been proposed in the field of psychophysics to quantify relationships between any stimulus and the perceived response by individuals. The Weber law asserts that the just noticeable stimulus difference  $\Delta I$  maintains a constant ratio with respect to the intensity of the comparison stimulus  $I$ . That is to say, if  $I$  is the intensity to which human eyes are adapted, and  $\Delta I$  the increase in that intensity which is just perceptible, then the ratio  $\frac{\Delta I}{I}$  may be considered as a measure of the discriminating power of human eyes. Furthermore, on the assumption that the difference threshold represents a unit change in sensation  $\Delta S$ , Fechner defined Weber's law as:

$$\Delta S = k \frac{\Delta I}{I} \quad (6)$$

Integrating this formula, a logarithmic relation called the psychophysical law is generated, as shown in Equation (7).

$$S = k \ln I + C \quad (7)$$

where  $k$  and  $C$  are hyper parameters,  $I$  denotes the magnitude of a physical stimulus and  $S$  denotes the corresponding perceived intensity. The Weber-Fechner law revealed the logarithmic mapping between the magnitude of a physical stimulus and its perceived intensity, rather than absolute magnitude value.

#### C. Texture Masking

According to texture masking theory [22], human eyes are more sensitive to perturbations on pixels in smooth regions than those in textured regions. We add  $3 \times 3$  window perturbations with 100 magnitudes in the smooth region and the textured region respectively for comparison of perceptual distance. Figure 4 plots the benign example, perturbed image at textured regions and perturbed image at smooth regions from left to right. When perturbations with the same magnitude are added to the image, the perturbations in smooth regions are easy to be detected by human eyes, while those in textured regions are difficult to be recognized.



Fig. 4. Perceptual distance of the perturbations with the same magnitude in different regions. The green line box marks perturbations in perturbed images. (a) benign example, (b) perturbed image at textured regions, (c) perturbed image at smooth regions.

The standard deviation is a commonly used quantity to measure the texture masking of an image, which is proved to be effective in evaluating the perceptual loss of adversarial examples. The paper computes the standard deviation of a pixel  $p_i$  among an  $n \times n$  window as shown in Equation (8).

$$SD(p_i) = \sqrt{\frac{\sum_{p_i \in S_i} (p_i - \mu)^2}{n^2}} \quad (8)$$

where  $S_i$  is the set consisting of pixels in the  $n \times n$  window,  $\mu$  is the average value of pixels in the region. The standard deviation  $SD(p_i)$  is the variance of a pixel  $p_i$  among  $S_i$ . In the paper, we set  $n = 3$  and calculate the standard deviation of the pixel  $p_i$  and its 8 neighbors. The texture masking reveals

the close relationship between the perceptual loss and the local texture feature of the image. The region with the high standard deviation could hide more perturbations in an image.

#### D. Channel Modulation

According to spectral sensitivity theory [23, 24], the brain computes visual color by analyzing the relative excitations of three types of retinal cones, which is a specialized light-sensitive cell found in the retina of the eye and used for discrimination of color. Human eyes consist of red, green and blue cone cells, cone sensitized to different ranges of wavelength to provide a range of color perception. Due to differences in the number of cone cells, the human eyes are the most sensitive to green, followed by red, and the least sensitive to blue. We conduct the perturbations with the same magnitude in three color channels respectively. As shown in Fig. 5, the test has proved just that.

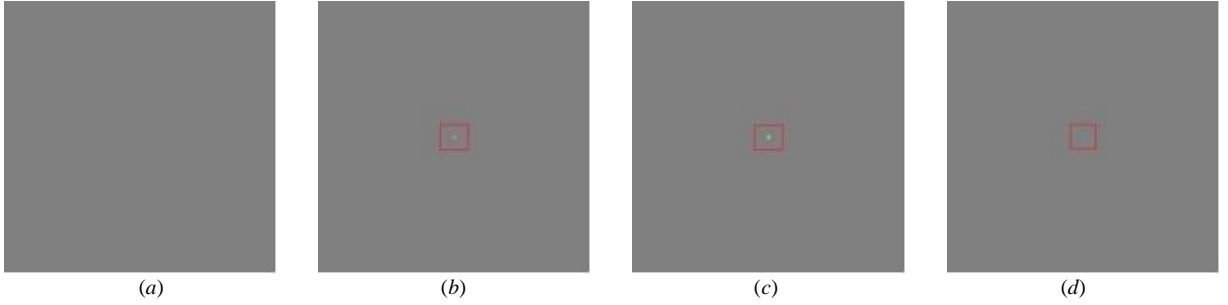


Fig. 5. Perceptual distance of the perturbations with the same magnitude in different channels. (a) benign example, (b) perturbed example in the red channel, (c) perturbed example in the green channel (d) perturbed example in the blue channel. The red Line box marks perturbations in perturbed examples.

The channel modulation is referred to a constrained linear combination of red, green and blue channels based on decolorization theory [24], which is formulated in Equation (9) for CIFAR-10.

$$\begin{aligned} \varpi &= \chi_r I_r + \chi_g I_g + \chi_b I_b \\ \text{s.t. } \chi_r + \chi_g + \chi_b &= 1 \\ \chi_r \geq 0, \chi_g \geq 0, \chi_b &\geq 0 \end{aligned} \quad (9)$$

where  $I_r$ ,  $I_g$  and  $I_b$  are input channels respectively, and  $\varpi$  is the result of the channel modulation. The non-negative numbers  $\chi_r$ ,  $\chi_g$  and  $\chi_b$  are channel weights that sum to 1. In the classical RGB2GRAY conversion model [24], the weights are fixed as  $\{\chi_r = 0.299, \chi_g = 0.587, \chi_b = 0.114\}$ . In fact, a more flexible scheme would be fixing channel weights depending on specific input images and individuals.

#### IV. METHODOLOGY

Adversarial example attacks could be formulated as an optimization problem with constrains. This problem involves the definition of the perceptual loss and the solution for the optimal problem. In the section, we describe in detail the definition of the perceptual loss integrating JND, Weber-Fechner law, texture masking, channel modulation and present a new method combining differential evolution with the greedy approximation to solve for the adversarial perturbations of images.

##### A. Perceptual Loss

In the investigation into the HVS, we find that the perceptual loss is primarily affected by four factors, namely JND, Weber-Fechner law, texture masking and channel

modulation. Weber-Fechner law reveals nonlinear relationships between any stimulus and the perceived response by individuals. In computer vision, the application of this law needs to consider the difference in perceived intensity of human eyes under different luminance backgrounds. The visibility of human eyes to perturbations of images has a positive correlation with stimulus and a negative correlation with JND. Thus, we combine Equation (5) and (6) to get a new quantity considering the perturbation intensity and the background luminance, as shown in Equation (10).

$$\Delta Ps = k \frac{\Delta I}{JND(I)} \quad (10)$$

where  $k$  is a constant according to Weber-Fechner law,  $\Delta I$  is the just noticeable stimulus difference and  $\Delta Ps$  is a corresponding change in visual sensation. Since  $JND(I)$  is a discrete piecewise function, we sum over the Equation (10) rather than integrate, as shown in Equation (11).

$$Ps(I) = k \sum_{i=I_0}^{I-1} \frac{1}{JND(i)} + C \quad (11)$$

where  $Ps(I)$  is perceptual stimulus and  $I_0$  is background luminance,  $k$  and  $C$  are constants. For the CIFAR-10 dataset, the pixel value ranges from 0 to 255 and the minimum difference between them is 1. For constructing the mapping between a physical stimulus and its perceptual stimulus, we define the perceptual stimulus in the interval  $[0, 255]$ . Obviously, a perturbation of magnitude 0 do not cause any perceptual perception to human eyes and a perturbation of magnitude 255 could cause the most noticeable perceptual perception. Thus, an equation could be constructed as follows to compute the constants  $k$  and  $C$ . That is,

$$\begin{cases} Ps(0) = C = 0, & \text{if } I = 0 \\ Ps(255) = k \sum_{i=0}^{255} \frac{1}{JND(i)} + C = 255, & \text{if } I = 255 \end{cases} \quad (12)$$

By solving the Equation (12), we get the parameter  $C = 0$  and  $k = \frac{256}{\sum_{i=0}^{255} \frac{1}{JND(i)}}$ .

Texture masking reflects that perturbations at the region with high standard deviation are more imperceptible for human eyes than low standard deviation. The visibility of human eyes to perturbations has a negative correlation with the standard deviation of the region in an image. Furthermore, taking channel modulation into consideration, the definition of the perceptual loss fixes color channel weights according to decolorization theory. Thus, we propose an integrated metric to evaluate the perceptual loss as follow.

$$IntegLoss(p_i) = \sum_{c \in (r, g, b)} \chi_c \frac{Ps_c(p_i)}{SD_c(p_i)} \quad (13)$$

Adversarial example attacks usually add multiple pixel perturbations for success rate. The perceptual loss between the benign image and the adversarial one is the sum of the all pixel-wise perceptual loss. Therefore, we sum up all pixel-wise perceptual loss as follow.

$$IntegLoss(X, X') = \sum_{i=1}^N \sum_{c \in (r, g, b)} \chi_c \frac{Ps_c(p_i)}{SD_c(p_i)} \quad (14)$$

where  $N$  is the number of perturbed pixels in a benign image.  $IntegLoss(X, X')$  denotes the perceptual loss integrating JND, Weber-Fechner law, texture masking and channel modulation between the benign example  $X$  and the adversarial one  $X'$ . The small  $IntegLoss$  value indicates the high perceptual similarity between the benign example and the adversarial one.

### B. Pixel-wise Objective Function

State-of-the-art adversarial example attacks should allow DNNs to give the wrong output with a high confidence score by adding as little perturbations as possible. Therefore, we should choose these pixels that can reduce the confidence of DNNs in the true class or increase that in the target class with the less perceptual loss. The pixel-wise objective function called perturbation priority is defined to estimate the effect of perturbing a pixel as follow.

$$PertPriority(p_i) = \zeta \frac{P_t(X) - P_t(X')}{IntegLoss(p_i)} \quad (15)$$

where  $P_t$  denotes the probability that the example belongs to the label  $t$ . The adversarial example  $X'$  is synthesized by changing a pixel  $p_i$  of the benign example  $X$ . When  $t = l$ , setting  $\zeta = 1$  and non-targeted attacks are executed, otherwise setting  $\zeta = -1$  and targeted attacks are executed. Perturbation priority quantify the effects of the current pixel  $p_i$  perturbation on the confidence of the DNNs-based classifier in the target class. The bigger values of the perturbation priority are, the greater effects of the perturbations are.

### C. Implementation

For finding out the pixels with high perturbation priority, the adversary has to choose which pixels to modify and what magnitudes to add for high misclassification ratio and low

imperceptibility metrics. We encode the pixel-wise perturbation into an array as candidate solution  $(x, y, r, g, b)$ , which contains five elements:  $x$ - $y$  coordinates and RGB value of the perturbation. A brute-force approach has to search all dimensions and pixel values for the optimal one. However, through this method the time taken for solving the problem is prohibitively long. Considering the time cost, we introduce the differential evolution referred in subsection II-E to solve the optimal of the pixel-wise objective function as the fitness function. To achieve a balance between the rich population and the fast running speed, for CIFAR-10 the GreedyFool sets the total population size to be 300 and the number of generations  $maxIter$  to be 60 for obtaining 18,000 candidate solutions with perturbation priority. And then the greedy approximation is utilized to automatically get a set of perturbed pixels and synthesize the imperceptible adversarial example. The detailed implementation of the GreedyFool is presented in Algorithm 1.

---

#### Algorithm 1: The Implementation of the GreedyFool

---

**Input:** The original image  $X$ , the initial parameters of the differential evolution

**Output:** Adversarial example  $X'$

```

1 for  $i = 0$  to  $maxIter$  do:
2   Calculate perturbation priority  $PertPriority$  of all
   candidate solutions by the differential evolution and obtain a set
    $Pp = \{(unit_1, PertPriority_1), (unit_2, PertPriority_2), \dots\}$ , where
    $unit_i = (x_i, y_i, r_i, g_i, b_i)$ 
3 end for
4 Sort  $Pp$  with  $PertPriority$  in descending order to obtain a set
    $Sp = \{(unit'_1, PertPriority'_1), (unit'_2, PertPriority'_2), \dots\}$ , where
    $unit'_i = \{x'_i, y'_i, r'_i, g'_i, b'_i\}$ 
5 for  $i = 0$  to  $maxIter$  do:
6    $units \leftarrow unit'_i$ 
7   if  $f(X) \neq f(X + units)$  do:
8     break
9   end if
10 end for
11  $X' = X + units$ 

```

---

## V. EXPERIMENTAL EVALUATION

In this section, we introduce the experimental setup in Section A. We evaluate the proposed GreedyFool from the aspects of imperceptibility (Section B), misclassification ratio (Section C), fitness convergence (Section D) and the running time (Section E) against ResNet and DenseNet.

### A. Experimental Setup

In this experiment, we implement the GreedyFool in Python and conduct the adversarial example attack in CIFAR-10 over ResNet and DenseNet presented in Section II-A. Due to the size  $32 \times 32$  and pixel value interval  $[0, 255]$  of images, the population of the differential evolution is initialized by uniform distributions  $U(1, 32)$  to generate  $x$ - $y$  coordinate and Gaussian distributions  $N(\mu = 128, \sigma = 127)$  for pixel RGB values. The fitness function of the differential evolution is set to pixel-wise objective function in Equation (15). The population size is 300 and the number of generations is 60. The weights of the channel modulation are fixed as  $\{\chi_r = 0.299, \chi_g = 0.587, \chi_b = 0.114\}$  for all test images based on the RGB2GRAY conversion model. The GreedyFool runs on an Intel Core I5 CPU 2.30 GHz, NVIDIA GeForce GTX



1060 and 8.0 GB of RAM computer running on Windows 10 and Spyder (Python 3.6).

### B. Imperceptibility

Imperceptibility refers to the indistinguishable distance by human eyes between benign examples and adversarial examples. We present 10 classes of images in Fig.6 and Fig.7, which include benign images and their corresponding adversarial images against ResNet and DenseNet models. Like the GreedyFool, both the One-pixel attack [22] and the PSD [31] attack belong to black-box attack using forward-propagation. Therefore, we carry out these three attacks on the same set of images to compare the imperceptibility of adversarial perturbations. Adversarial examples from the GreedyFool are listed in the second row. The following rows are adversarial examples synthesized by One-pixel attack and PSD methods.

As shown in Fig.6 and Fig.7, adversarial examples synthesized by the GreedyFool are much more imperceptible than other pixel-wise methods, which are higher perceptual similarity to correspondingly benign images. The PSD attack in the last row performs slightly worse results. The One-pixel attack in the third row performs the worst that human eyes

easily detect the perturbed pixels. TABLE III lists *IntegLoss* results of adversarial examples generated by these three methods. The results demonstrate that the GreedyFool could generate adversarial examples with smaller *IntegLoss* values than the PSD attack and the One-pixel attack, which are consistent with what human eyes perceive.

TABLE IV lists the perceptual distance results of adversarial examples generated by the GreedyFool in Fig.6 and Fig.7. The results show that  $L_p$  norms cannot always accurately quantify imperceptibility of adversarial perturbations. The proposed perceptual distance *IntegLoss* is more accurate than  $L_p$  norms to reflect perceptual similarity between the benign example and the adversarial one.

Among the three types of attack methods, the One-pixel attack hardly takes the HVS into consideration. The PSD attack considers the intensity and texture masking of benign images. The greedyFool combines JND, Weber-Fechner law, texture masking with color channel modulation to construct objective function of adversarial example attacks, giving full consideration to the HVS. The experimental results show the imperceptibility of adversarial examples could be further improved by combining multiple HVS metrics.

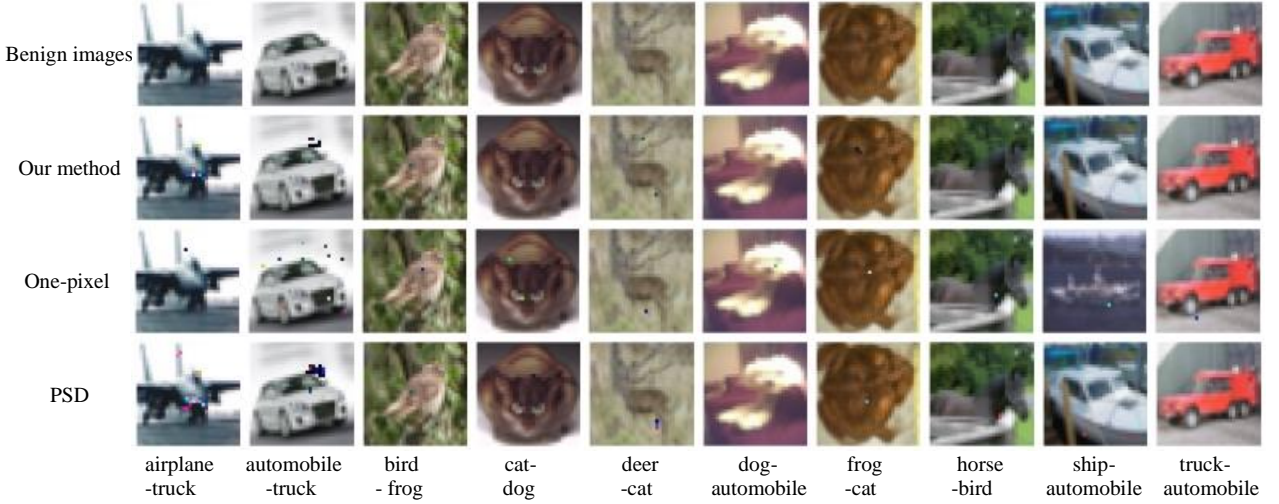


Fig. 6. Adversarial images synthesized by different attack methods against ResNet model in CIFAR-10. Adversarial examples in the second row crafted by our method are much more imperceptible than others from the following rows.

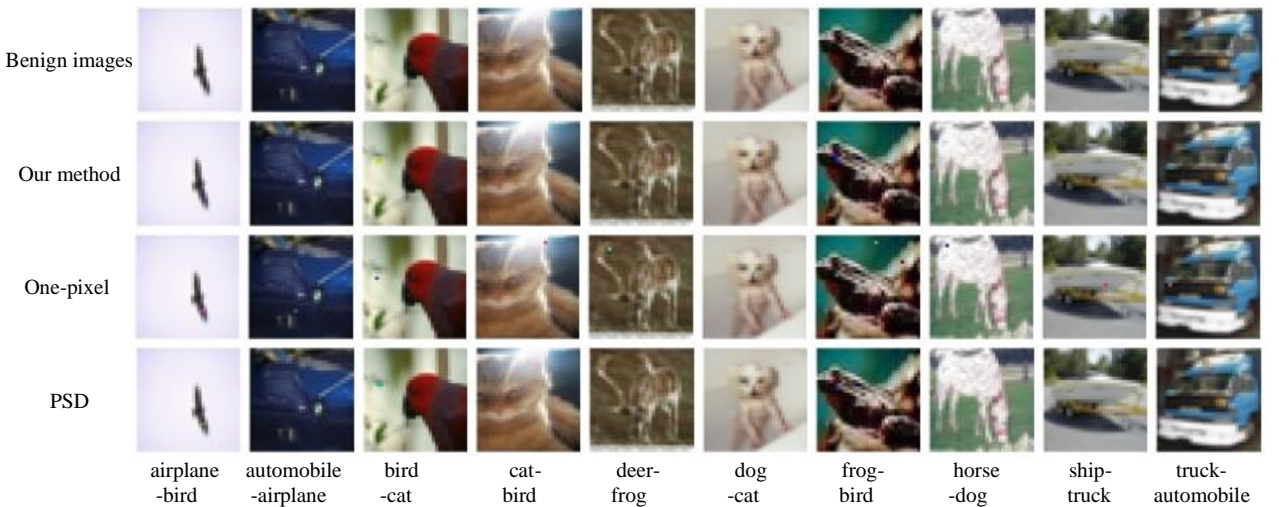


Fig. 7. Adversarial images synthesized by different attack methods against ResNet model in CIFAR-10. Adversarial examples in the second row crafted by our method are much more imperceptible than others from the following rows.

TABLE III. THE PROPOSED PERCEPTUAL DISTANCE RESULTS OF ADVERSARIAL EXAMPLES IN FIGURES 6 AND 7

Networks	Method	airplane	automobile	bird	cat	deer	dog	frog	horse	ship	truck
ResNet	[22]	159.9725	680.6277	9.2656	7.4370	15.1543	8.9546	27.4190	16.3758	42.7534	23.9218
	[31]	49.3604	392.8105	6.0965	3.0108	23.1974	0.0123	12.1553	0.7286	3.1867	0.2651
	Our	35.6880	317.2337	2.9297	1.0145	25.5201	0.0027	11.4457	0.7147	3.0271	0.2397
DenseNet	[22]	2.9803	24.6410	11.0931	7.8807	7.3199	4.0381	10.8706	7.0604	13.9815	7.1886
	[31]	1.3220	0.0145	3.4483	2.4777	0.6707	0.5324	2.8408	0.2824	0.1785	0.1701
	Our	0.3427	0.0058	2.4050	0.6525	0.3950	1.0061	1.5546	0.1475	0.0397	0.0647

TABLE IV. THE PERCEPTUAL DISTANCE RESULTS OF ADVERSARIAL EXAMPLES IN THE SECOND ROW IN FIGURES 6 AND 7

Networks	perceptual distance	airplane	automobile	bird	cat	deer	dog	frog	horse	ship	truck
ResNet	$L_0$	11	16	1	1	2	1	1	1	1	1
	$L_2$	1871	5637	136	57	296	1	264	211	108	42
	$L_\infty$	198	253	136	57	151	1	236	211	94	42
	IntegLoss	35.6880	317.2337	2.9297	1.0145	25.5201	0.0027	11.4457	0.7547	3.4271	0.2397
DenseNet	$L_0$	1	1	2	1	1	1	2	1	1	1
	$L_2$	210	2	397	125	69	93	462	75	5	47
	$L_\infty$	210	2	203	125	69	72	247	75	5	47
	IntegLoss	0.3427	0.0058	2.4050	0.6525	0.3950	1.0061	1.5546	0.1475	0.0397	0.0647

### C. Misclassification Ratio

According to the purpose of tasks, adversarial example attacks can be classified as non-targeted attacks and targeted attacks. Non-targeted attacks aim to mislead DNN models to classify images into any wrong classes, while targeted attacks aim to mislead DNN models to classify images into a specific target class. The misclassification ratio is the most important property for adversarial example attacks. For non-targeted attacks, the misclassification ratio is formulated in Equation (16).

$$MR_{UA} = \frac{1}{N} \sum_{i=1}^N count(l \neq l') \quad (16)$$

where the function *count* is used to count the number of  $X'$  that is classified into the wrong class by deep learning.  $l$  and  $l'$  are labels of the benign example  $X$  and the adversarial one  $X'$  respectively. For targeted attacks, the misclassification ratio is formulated in Equation (17).

$$MR_{TA} = \frac{1}{N} \sum_{i=1}^N count(l = t) \quad (17)$$

where the adversarial example  $X'$  is classified into the target class  $t$ . we test 1000 random images and compare the misclassification ratio between the GreedyFool and two previous works. The results demonstrate that the GreedyFool achieves 100% success rate for non-targeted attacks and targeted attacks. In fact, as long as the perturbations are sufficient, any images could be recognized as a specified target class by deep learning. However, not all adversarial example attacks could achieve 100% success rate because some of them need to set the box-constrained parameters and generate adversarial examples under these constraints. For example, the one-pixel attack [22] needs to specify the number of disturbed pixels and the PSD attack [31] needs to set the max human perceptual distance. When the number of disturbed pixels is set to 5, success rate of the one-pixel attack may achieve 86% for non-targeted attacks and 44% for targeted attacks. Success rate of the PSD attack may achieve 84% for non-targeted attacks and 72% for targeted attacks under the max human perceptual distance. It is difficult to find out appropriate box-constrained parameters before adversarial example attacks on a specific image. The strict constraints may result in unsuccessful adversarial example attacks while the loose constraints may allow human eyes to detect the

perturbations easily. Our attack method utilizes the greedy approximation to obtain approximately the least visible perturbations without setting box-constrained parameters, which could automatically generate the imperceptible adversarial examples in 100% success rate.

### D. Convergence of Fitness Function

The running speed of the GreedyFool largely depends on the convergence of the differential evolution. The fitness function is set to be the pixel-wise objective function called perturbation priority as defined in Equation (15). The goal of the differential evolution is to maximize this fitness value. We conduct an experiment on ResNet and DenseNet model to examine how the fitness changes during evolution. Figures 8 shows their fitness convergences of 30 random images during 60 generations.

As shown in Fig.8, each line plots the fitness convergence of an image. Some images could find the highest-priority perturbation pixel with a low number of generations, while others require a sufficient number of generations. Over both ResNet and DenseNet, fitness function eventually converges on a stable state after about 50 generations. It is proved that the differential evolution is a feasible approach to solve for pixels with high perturbation priority.

### E. Computation Cost

Computation cost refers to the running time for attackers to synthesize an adversarial example, which is used to evaluate the attack time cost. The computation cost of the GreedyFool is affected by several factors, including the feedback time of the DNN model, convergence speed of the differential evolution, the number of the greedy approximation, running environment, etc. Because the GreedyFool utilizes the feedback of the deep neural network to guide the evolution direction of the adversarial perturbations, our experiment chooses 30 random images from CIFAR-10 to test the actual running time of the DNNs and the GreedyFool towards these DNNs. The running time of ResNet and DenseNet is plotted in Fig.9. The average running time of ResNet is 0.008346 seconds while that of DenseNet is 0.015876 seconds. The GreedyFool running time towards ResNet and DenseNet is plotted in Fig.10. On average, the GreedyFool takes about 14.943498 seconds towards ResNet



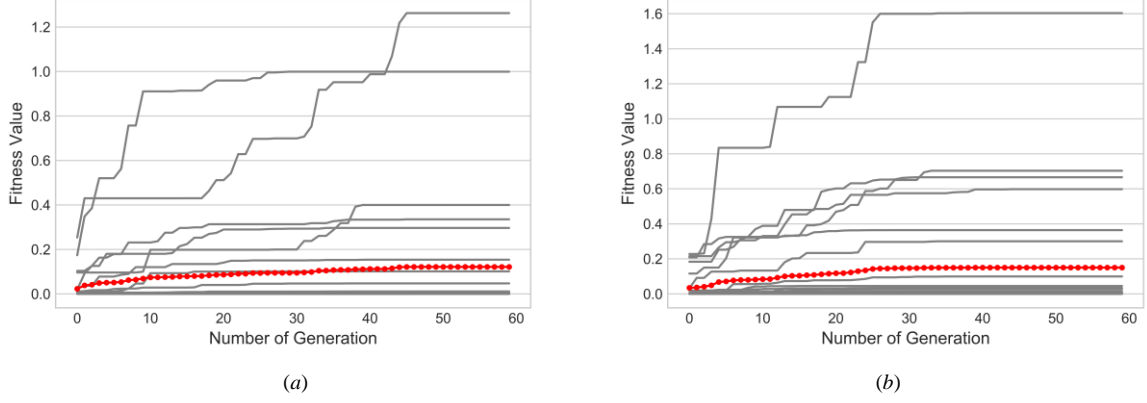


Fig. 8. Fitness convergence tests. (a) convergence of fitness function over ResNet, (b) convergence of fitness function over DenseNet. The average values are highlighted by red dotted lines.

and 38.444529 seconds towards DenseNet to synthesize an adversarial example.

The comparison between Figures 9 and 10 reveals that the running time of the GreedyFool is not completely consistent with that of the corresponding DNN. But in general, The GreedyFool shows higher attack efficiency for such neural networks that can feedback probability labels in a short time.

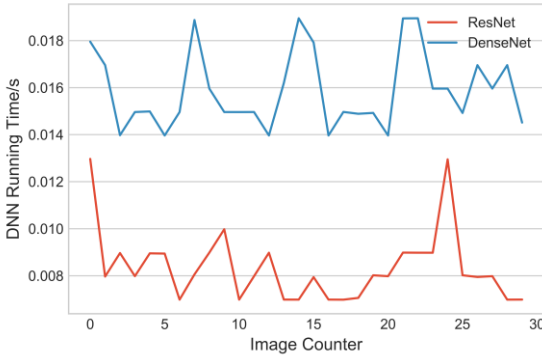


Fig. 9. Fitness convergence tests. (a) convergence of fitness function over ResNet, (b) convergence of fitness function over DenseNet. The average values are highlighted by red dotted lines.

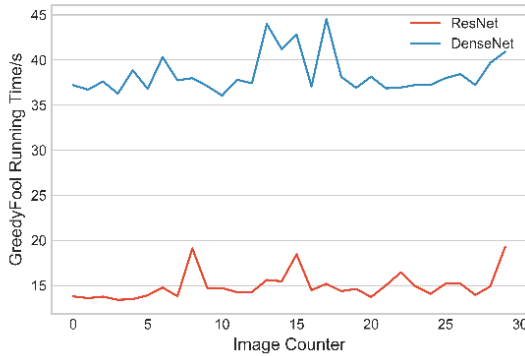


Fig. 10. Fitness convergence tests. (a) convergence of fitness function over ResNet, (b) convergence of fitness function over DenseNet. The average values are highlighted by red dotted lines.

## VI. DISCUSSION

Previous works have analyzed the advantages of the differential evolution in the pixel-wise adversarial example attack [22]. In the paper, we propose a new adversarial

example attack combining the differential evolution and the greedy approximation using forward-propagation. The differential evolution is utilized to obtain a large number of candidates with high perturbation priority by generationally solving for optimization. And based on the greedy approximation, the proposed method selects pixels with the current highest perturbation priority from candidates to synthesize the less noticeable adversarial examples. To properly define the perceptual loss, we launch a lot of investigations into the HVS and design an integrated metric considering four primary factors affecting the perception of perturbations by human eyes, including JND, Weber-Fechner law, texture masking and channel modulation. Our work has mainly the following remarkable properties:

(1) Black-box attack. The GreedyFool attacks DNN models depending on only their probability labels but no inner information of target DNNs, such as gradients, network structures, etc.

(2) Imperceptibility. The definition of the perceptual loss takes JND, Weber-Fechner law, texture masking and channel modulation of the HVS into consideration, which introduces a comprehensive metric covering background luminance, nonlinear mapping of intensity, local texture feature and spectral sensitivity to evaluate the perceptual distance.

(3) Success rate. The GreedyFool outperforms the state-of-the-art pixel-wise methods in the misclassification ratio, which achieves 100% success rate for both non-targeted attacks and targeted attacks.

(4) Flexibility. Rather than several gradient-based algorithms, the proposed algorithm based on differential evolution does not use the gradient information of neural network, so it can attack more types of DNN model even if their gradients are not differentiable.

(5) Automation. The GreedyFool automatically synthesize the less perceptible adversarial examples based on the greedy approximation without setting box-constrained parameters.

## VII. CONCLUSION

Adversarial example attacks against neural networks are a serious threat for the safety-critical systems. In this paper, we propose a novel approach GreedyFool based on the differential evolution and the greedy approximation to generate adversarial examples using forward-propagation. The GreedyFool evaluates the effects of pixel-wise

perturbations and generates the candidate pixels with the higher perturbation priority by the differential evolution. And the greedy approximation is used to get the proper perturbations from candidates to automatically synthesize the imperceptible adversarial examples. The proposed method could attack more types of DNNs depending on only their probability labels. In the definition of the perceptual loss, existing works lack sufficient consideration of the HVS, resulting in noticeable artifacts. We further launch a lot of investigations into the HVS and introduce a integrated metric to define the perceptual loss from background luminance, nonlinear mapping of intensity, local texture feature and spectral sensitivity. We implement the GreedyFool and conduct the adversarial example attack in CIFAR-10 over ResNet and DenseNet. The experimental results demonstrate its much more imperceptibility than that of the state-of-the-art pixel-wise methods and its 100% success rate. Furthermore, we test the convergence of fitness function and computation cost to prove the feasibility of the proposed method.

## REFERENCES

- [1] X. Yuan, P. He, Q. Zhu and X. Li, "Adversarial examples: Attacks and defenses for deep learning", *IEEE Transactions on Neural Networks and Learning Systems*, vol. 30, no. 9, pp. 2805-2824, 2019.
- [2] K. He, X. Zhang, S. Ren, and J. Sun, "Deep residual learning for image recognition", *IEEE Conference on Computer Vision and Pattern Recognition (CVPR)*, pp. 770-778, 2016.
- [3] G. Huang, Z. Liu, L. Maaten, and K. Weinberger, "Densely connected convolutional networks", *IEEE Conference on Computer Vision and Pattern Recognition (CVPR)*, pp. 4700-4708, 2017.
- [4] S. Horiguchi, S. Amano, M. Ogawa and K. Aizawa, "Personalized classifier for food image recognition", *IEEE Transactions on Multimedia*, vol. 20, no. 10, pp. 2836-2848, 2018.
- [5] X. Dong, J. Shen, D. Wu, W. Wang, and F. Porikli, "Quadruplet network with one-shot learning for fast visual object tracking", *IEEE Transactions on Image Processing*, vol. 28, no. 7, pp. 3516-3527, 2019.
- [6] J. Li, S. Ji, T. Du, B. Li and T. Wang, "Textbugger: generating adversarial text against real-world applications", *Network and Distributed System Security Symposium (NDSS)*, pp. 1-15, 2019.
- [7] T. Young, D. Hazarika, S. Poria and E. Cambria, "Recent trends in deep learning based natural language processing", *IEEE Computational Intelligence Magazine*, vol. 13, no. 3, pp. 55-75, 2018.
- [8] Y. Qin, N. Carlini, G. Cottrell, I. Goodfellow and C. Raffel, "Imperceptible, robust, and targeted adversarial examples for automatic speech recognition", *Proceedings of Machine Learning Research (PMLR)*, pp. 5231-5240, 2019.
- [9] A. Graves, A. Mohamed and G. Hinton, "Speech recognition with deep recurrent neural networks", *IEEE International Conference on Acoustics, Speech and Signal Processing (ICASSP)*, pp. 6645-6649, 2013.
- [10] A. Chakraborty, M. Alam, V. Dey, A. Chattopadhyay, and D. Mukhopadhyay, "Adversarial attacks and defenses: a survey". *arXiv preprint arXiv: 1810.00069*, 2018.
- [11] H. Xu, Y. Ma, H-C. Liu, D. Deb, H. Liu, J-L, T and A. Jain, "Adversarial attacks and defenses in images, graphs and text: a review", *International Journal of Automation and Computing*, vol. 17, no. 2, pp. 151-178, 2019.
- [12] C. Szegedy, W. Zaremba and I. Sutskever, "Intriguing properties of neural networks", *arXiv preprint arXiv: 1312.6199*, 2013.
- [13] I-J. Goodfellow, J. Shlens, and C. Szegedy, "Explaining and harnessing adversarial examples", *arXiv preprint arXiv: 1412.6572*, 2014.
- [14] M. Sharif, S. Bhagavatula, L. Bauer L and M. Reiter, "Accessorize to a crime: real and stealthy attacks on state-of-the-art face recognition", *ACM Conference on Computer and Communications Security (CCS)*, pp. 1528-1540, 2016.
- [15] H. Wang, D. Gong, Z. Li and W. Liu, "Decorrelated adversarial learning for age-invariant face recognition", *IEEE Conference on Computer Vision and Pattern Recognition (CVPR)*, pp. 3527-3536, 2019.
- [16] E. Quiring, D. Arp and K. Rieck, "Forgotten siblings: Unifying attacks on machine learning and digital watermarking", *IEEE European Symposium on Security and Privacy (EuroS&P)*, pp. 488-502, 2018.
- [17] J. Hayes, "On visible adversarial perturbations and digital watermarking", *IEEE Conference on Computer Vision and Pattern Recognition Workshops (CVPR)*, pp. 1597-1604, 2018.
- [18] Z. Dou, S. Osher and B. Wang, "Mathematical analysis of adversarial attacks", *arXiv preprint arXiv: 1811.06492*, 2018.
- [19] B. Rouani, M. Samragh, T. Javidi and F. Koushanfar, "Safe machine learning and defeating adversarial attacks", *IEEE Symposium on Security and Privacy (S&P)*, pp. 31-38, 2019.
- [20] N. Papernot, P. McDaniel, I. Goodfellow, S. Jha, Z-B. Celik and A. Swami, "Practical black-box attacks against machine learning", *ACM Conference on Computer and Communications Security (CCS)*, pp. 506-519, 2017.
- [21] N. Papernot, P. McDaniel, S. Jha, M. Fredrikson, Z-B Celik and A. Swami, "The Limitations of deep learning in adversarial settings", *IEEE European Symposium on Security and Privacy (EuroS&P)*, pp. 372-387, 2016.
- [22] J. Su, D-V. Vargas and K. Sakurai, "One pixel attack for fooling deep neural networks", *IEEE Transactions on Evolutionary Computation*, vol. 23, no. 5, pp. 828-841, 2019.
- [23] S-M Moosavi-Dezfooli, A. Fawzi and P. Frossard, "Deepfool: a simple and accurate method to fool deep neural networks", *IEEE Conference on Computer Vision and Pattern Recognition (CVPR)*, pp. 2574-2582, 2016.
- [24] Y. Liu, X. Chen, C. Liu and D. Song, "Delving into transferable adversarial examples and black-box attacks", *International Conference on Learning Representations (ICLR)*, pp. 1-14, 2017.
- [25] N. Carlini and D. Wagner, "Towards evaluating the robustness of neural networks", *IEEE Symposium on Security and Privacy (S&P)*, pp. 39-57, 2017.
- [26] N. Carlini, G. Katz, C. Barrett and D-L. Dill, "Provably minimally-distorted adversarial examples", *arXiv preprint arXiv: 1709.10207*, 2017.
- [27] X. Yang, W. Ling, Z. Lu, E. Ong, and S. Yao, "Just noticeable distortion model and its applications in video coding", *Signal Processing: Image Communication*, vol. 20, no. 7, pp. 662-680, 2005.
- [28] Z. Wang, M. Song, S. Zheng, Z. Zhang, Y. Song and Q. Wang, "Invisible adversarial attack against deep neural networks: An adaptive penalization approach", *IEEE Transactions on Dependable and Secure Computing*, DOI: 10.1109/TDSC.2019.2929047.
- [29] J. Drosler, "An n-dimensional Weber law and the corresponding Fechner law", *Journal of Mathematical Psychology*, col. 44, no. 2, pp. 330-335, 2020.
- [30] S. Dehaene, "The neural basis of the Weber-Fechner law: A logarithmic mental number line", *Trends in Cognitive Sciences*, col. 7, no. 4, pp. 145-147, 2003.
- [31] B. Luo, Y. Liu, L. Wei and Q. Xu, "Towards imperceptible and robust adversarial example attacks against neural networks", *AAAI Conference on Artificial Intelligence (AAAI)*, pp. 1-8, 2018.
- [32] J-L. Schnapf, T-W. Kraft and D-A. Baylor, "Spectral sensitivity of human cone photoreceptors", *Nature*, col. 325, no. 6103, pp. 439, 1987.
- [33] Y. Song, L. Bao and X. Xu, "Decolorization: Is rgb2gray () out?", *International Conference on Computer Graphics and Interactive Techniques (SIGGRAPH)*, pp. 15, 2013.
- [34] P. Civicioglu and E. Besdok, "A conceptual comparison of the cuckoosearch, particle swarm optimization, differential evolution and artificial bee colony algorithms". *Artificial Intelligence Review*, 2013: 1-32.
- [35] X. Zhou, C. Peng, J. Liu, Y. Zhang and G-J Zhang, "Underestimation-assisted global-local cooperative differential evolution and the application to protein structure prediction", *IEEE Transactions on Evolutionary Computation*, col. 24, no. 3, pp. 536-550, 2020.
- [36] Z. Zhan, Z. Wang, H. Jin and J. Zhang, "Adaptive distributed differential evolution". *IEEE Transactions on Cybernetics*, col. 10, pp. 1-15, 2019.